Computational Analysis of Two-Dimensional Flows with OpenFOAM

Robert D. Habbit, III[1], Andrew B. Porteus[2], Carlos M. Lazaro Echavarria[3], Svetlana V. Poroseva[4]
The University of New Mexico, Albuquerque, New Mexico, 87131

and

Scott M. Murman[5]
NASA Ames Research Center, Moffett Field, CA 94035

In this paper, results of incompressible turbulent flow simulations around a two-dimensional NACA 4412 airfoil at different angles of attack and a two-dimensional circular cylinder are presented. Simulations were conducted with Wilcox's 2006 k-ω and Menter's SST turbulence models, as well as the Launder-Reece-Rodi Reynolds Stress Transport model implemented in open-source OpenFOAM software. Results of simulations are compared with those obtained with the NASA CFL3D and FUN3D codes and with experimental, LES, DES, and URANS data when available.

Nomenclature

Re	=	Reynolds Number, $U_\infty \rho / \nu$
M	=	Mach Number, U_∞ / a
ρ	=	Density
a	=	Speed of sound
U_∞	=	Free stream velocity
U	=	Velocity vector
u	=	Velocity in the streamwise direction
v	=	Velocity in the transverse direction
ν	=	Kinematic viscosity
μ	=	Dynamic viscosity
c	=	Chord
C_p	=	Pressure coefficient
C_f	=	Surface friction
D	=	Diameter of cylinder
L_r	=	Recirculation length of separation bubble
α	=	Angle of attack
θ	=	Angle on the cylinder from the stagnation point
ϕ	=	Separation angle
ε	=	Turbulent scalar dissipation ($= \frac{1}{2}\varepsilon_{kk}$)
k	=	Turbulent kinetic energy

---

[1] Graduate Student, Mechanical Engineering, MSC01 1105, 1 UNM Albuquerque, NM, 87131-00011, AIAA Student Member.

[2] Graduate Student, Mechanical Engineering, MSC01 1105, 1 UNM Albuquerque, NM, 87131-00011, AIAA Student Member.

[3] Graduate Student, Mechanical Engineering, MSC01 1105, 1 UNM Albuquerque, NM, 87131-00011, AIAA Student Member.

[4] Assistant Professor, Mechanical Engineering, MSC01 1105, 1 UNM Albuquerque, NM, 87131-00011, AIAA Associate Fellow.

[5] Aerospace Engineer, NASA Ames Research Center, Moffett Field, CA 94035.

ω	$=$	Turbulent specific dissipation, ε/k
v_t	$=$	Turbulent viscosity
y	$=$	Distance between a wall and the first grid node
β_1	$=$	Blending constant
L	$=$	Length of computational domain
R_{ij}	$=$	Reynolds stress tensor, $<u_i u_j>$
S_{ij}	$=$	Rate of strain tensor, $\frac{1}{2}\left(\frac{\partial U_i}{\partial x_j}+\frac{\partial U_j}{\partial x_i}\right)$
τ_w	$=$	Wall shear stress
u_τ	$=$	Friction velocity $\sqrt{\tau_w/\rho}$
y^+	$=$	Dimensionless distance from the wall based on fluid properties, yu_τ/v
$\vec{n}$	$=$	Normal vector to the surface
N	$=$	Total number of nodes in the computational domain
h	$=$	Characteristic mesh length for the constant domain size, $1/\sqrt{N}$

I.   Introduction

THE purpose of our study is two-fold: i) to evaluate the capabilities of open-source OpenFOAM software in predicting incompressible two-dimensional (2D) turbulent flows with separation around streamlined bodies such as the NACA 4412 airfoil[1] and a circular cylinder, and ii) to generate the reference database with standard turbulence models for these two flows. Simulations around the airfoil are conducted at the angles of attacks characteristic for the separation bubble formation in such a flow.

Standard turbulent models are those adopted by industry. They are one- and two-equation models that are known for not adequately predicting flow separation[2-5]. However, they allow for conducting fast computations of complex three-dimensional high-Reynolds-number flows and are applicable throughout the flight envelope. This explains their popularity. Second- and higher-order statistical closures based on the Reynolds-averaged Navier-Stokes (RANS) equations have more potential to accurately describe physics of complex turbulent flows, but are more challenging in their implementation. They also require more detailed modeling of physical processes that occur in turbulent flows. Modeling assumptions may affect the accuracy of flow predictions with higher-order closures.

In the current paper, simulation results in a flow around the NACA 4412 airfoil obtained with two-equation turbulence models – Wilcox's 2006 k-ω model[6,7] and Menter's SST model[8] – are compared with those obtained with two versions of the Launder-Reece-Rodi (LRR) Reynolds Stress Transport model[9] with the Gibson-Launder wall corrections[10] as described in Refs. 11 and 12. The same two-equation models are used for simulating a flow around a circular cylinder. In a flow around the airfoil, the results are compared with those obtained with the high-fidelity NASA codes, CFL3D and Flow3D[13] and experimental data[14-16]. Large-eddy simulations (LES) data are also available for this geometry[17]. In the cylinder flow, results obtained with the two-equation turbulence models are compared with the data from experiments[18], unsteady RANS (URANS)[19,20] simulations, LES[20], and Detached-eddy simulations[21,22] (DES).

II.   Computational Methods

The OpenFOAM[12] solver chosen for the problem is the semi-implicit method for pressure-linked equations (SIMPLE) algorithm. The SIMPLE algorithm solves iteratively for the velocity and pressure fields from predefined initial conditions in steady flow simulations. The discretization scheme applied is the second-order Gaussian integration scheme. The interpolation schemes are first-order linear approximations, except for the divergence scheme which uses upwind approximations. For the Laplacian scheme, the surface normal gradient scheme is chosen, which is a corrected unbounded second-order conservative scheme.

III.   Computational Domain

A. Grids

The computational domain used for the NACA 4412 simulations is a structured C-type mesh (Fig. 1), which was generated at NASA and is available at Turbulence Model Benchmarking Working Group's website[13]. The far field boundaries of the computational domain for this geometry are a hundred times the cord length away. Four grids with different refinement were used in our study: 113×33 with 65 points placed along the airfoil surface, 225×65 with

129 points along the airfoil surface, 449×129 with 257 points along the airfoil surface, and 897×257 with 513 points along the airfoil surface. The finest grid has the first computational node at y+ between 0.2 and 0.4. Each coarser grid corresponds to every other point from the previous finer grid.

For the cylinder flow simulations, the structured grid of the O-type was used (Fig. 2). The far field boundaries are placed 100 cylinder diameters away from the cylinder surface. There are 500 points along the cylinder surface and 460 points in the radial direction. Due to that fact that the domain is O-type, the far field boundaries have 250 points on the inlet and outlet. The grid contains 230,000 cells with the first computational node from the cylinder surface being at y^+~2 based on the experimental flow parameters in Achenbach[18].

a)   b)
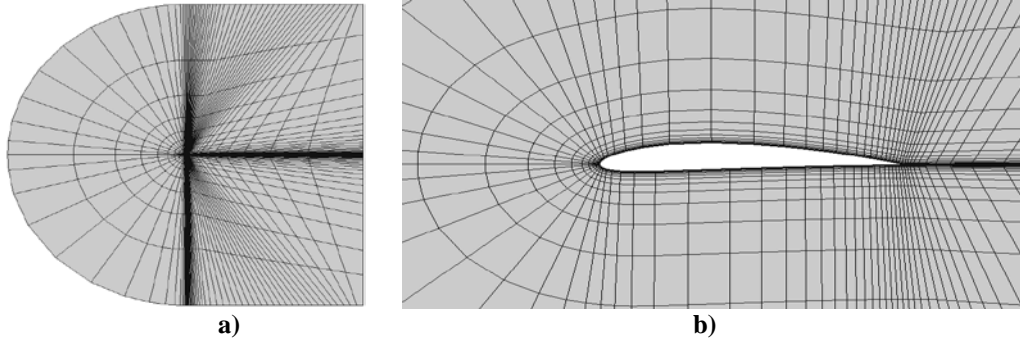
Figure 1. Grid 113 x 33 for the NACA 4412 airfoil (65 points on the airfoil surface): a) complete computational domain, b) zoomed view of the grid near the airfoil surface.
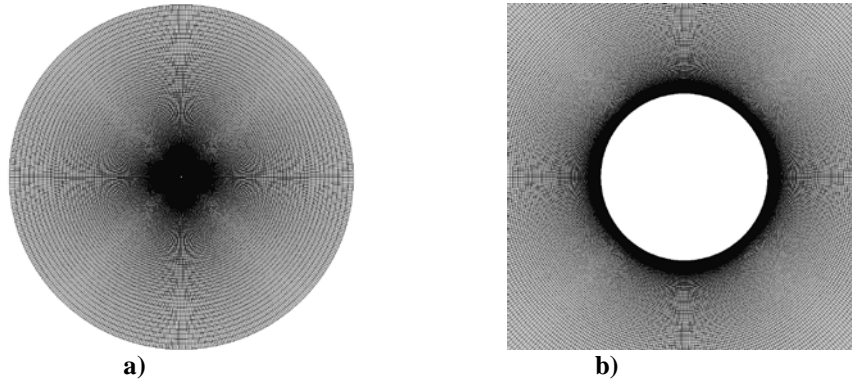

a)   b)

Figure 2. Computational domain for the 2D cylinder a) complete computational domain, b) zoomed view of the grid near the airfoil surface.

B. Boundary and Initial Conditions

In the simulations for the NACA 4412 airfoil, two separate sets of flow parameters were used. The first set contains the same parameters as in the simulations conducted at NASA Langley[13] and in the experiments conducted by Wadcock and Coles[14,15]. For this set, the inlet velocity magnitude corresponds to M = 0.09 and viscosity defined from the simulation at Re = 1.52×10⁶. The velocity direction is at α =13.87˚ to reproduce the angle of attack from the experiments[14,15]. The second set of flow parameters is based on more recent experiments conducted by Wadcock[16]: M = 0.085, Re = 1.64×10⁶ and α =12˚.

The initial internal velocity field is the same as at the inlet. The outlet boundary conditions are set to be the zero gauge pressure outlet. This is also the initial conditions for the internal pressure field. On the airfoil surface, the no-slip boundary condition is applied. The initial condition for the turbulent kinetic energy[13] is:

$$k_{farfield} = \frac{3}{20}(U_\infty I)^2 \qquad (1)$$

The initial conditions for the specific dissipation rate[13] are:

$$\omega_{wall} = 10\frac{6\nu}{\beta_1 y^2}, \qquad \omega_{farfield} = 1 \times 10^{-6}\frac{\rho_\infty a_\infty^2}{\mu_\infty}. \tag{2}$$

For the flow simulations around a cylinder, the initial conditions correspond to those in the experiments[18] and used in URANS[19] and DES[21,22]. The initial velocity field and the velocity inlet conditions correspond to the Mach number M = 0.09 and viscosity defined from simulations at the Reynolds number based on the cylinder diameter of 3×10^6 and 3.6×10^6. The outlet condition and the initial pressure field are set to the zero gage pressure. On the cylinder surface, the no-slip smooth surface boundary condition is applied. Initial conditions for the turbulent kinetic energy and the specific dissipation rate are given by Eqs. (1) and (2) .

IV. Results

A. NACA 4412
A sensitivity analysis of the simulation results to the grid refinement was performed for the NACA 4412 airfoil. Four different grids and two turbulence models in their standard formulations[13] – Wilcox's 2006 k-ω model[6,7] and Menter's SST model[8] – were used in this study. Figures 3 and 4 show the convergence of the streamwise velocity profiles at six locations, while Figs. 5 and 6 show the convergence of the transverse velocity profiles for the k-ω model[6,7] and Menter's SST model[8], respectively.

Figures 7 and 8 show the convergence of results for the pressure coefficient and the skin friction coefficient obtained with the two turbulence models. The largest differences between the solutions obtained with different grids are observed near the trailing edge where the flow separation occurs.

The characteristic mesh length, h, for the constant domain size is used in our study to analyze the grid resolution effects on the solutions obtained with different turbulence models. The results are shown in Figs. 9 and 10.The skin friction coefficient and the pressure coefficient were considered at two locations: one towards the leading edge of the airfoil and the other in the recirculation zone at the trailing edge of the airfoil.

In Figures 11-13, results obtained with the two-equation turbulence models implemented in OpenFOAM[12] are compared with the data obtained with the CFL3D and FUN3D codes[13]. Figures 11 and 12 show the streamwise and transverse velocities. Variations of the pressure coefficient along the airfoil surface are given in Fig. 13.
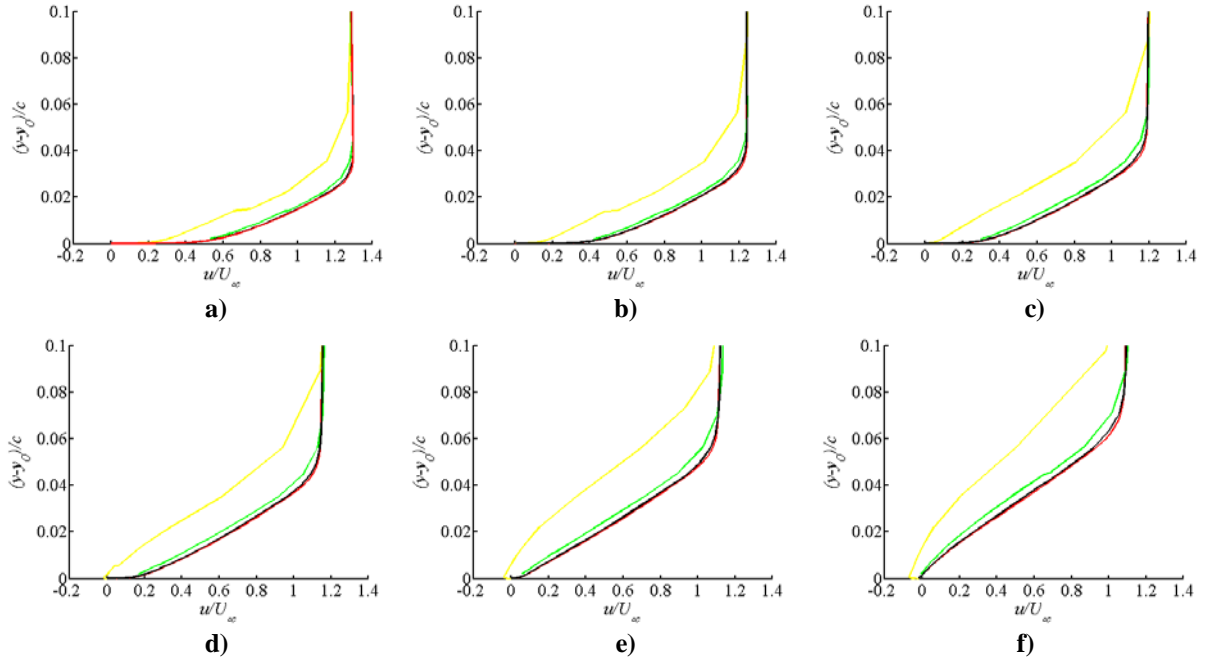

Figure 3. The streamwise velocity profiles at a) x/c =0.6753, b) x/c =0.7308, c) x/c=0.7863, d) x/c=0.8418, e) x/c=0.8973 and, d) x/c=0.9528 obtained with the k-$\omega^{6,7}$ model on different grids: —— 113×33, —— 225×65, —— 449×129, —— 897×257.
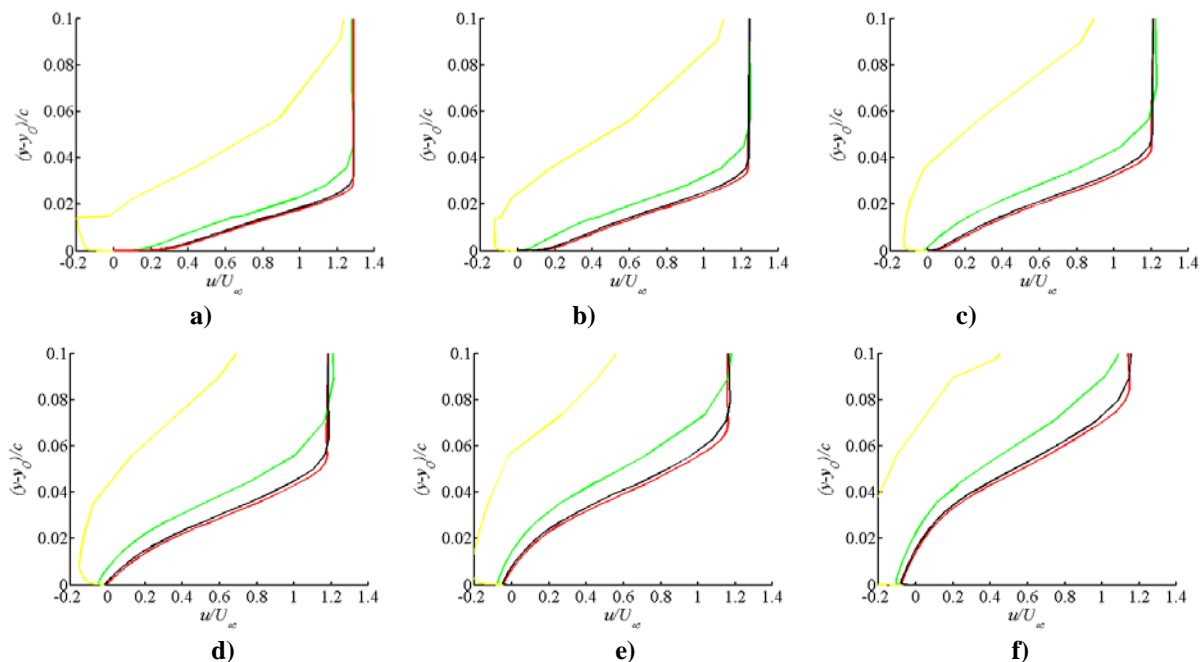
Figure 4. The streamwise velocity profiles at a) x/c =0.6753, b) x/c =0.7308, c) x/c=0.7863, d) x/c=0.8418, e) x/c=0.8973 and, d) x/c=0.9528 obtained with Menter's SST model[8] on different grids (notations as in Fig. 3).
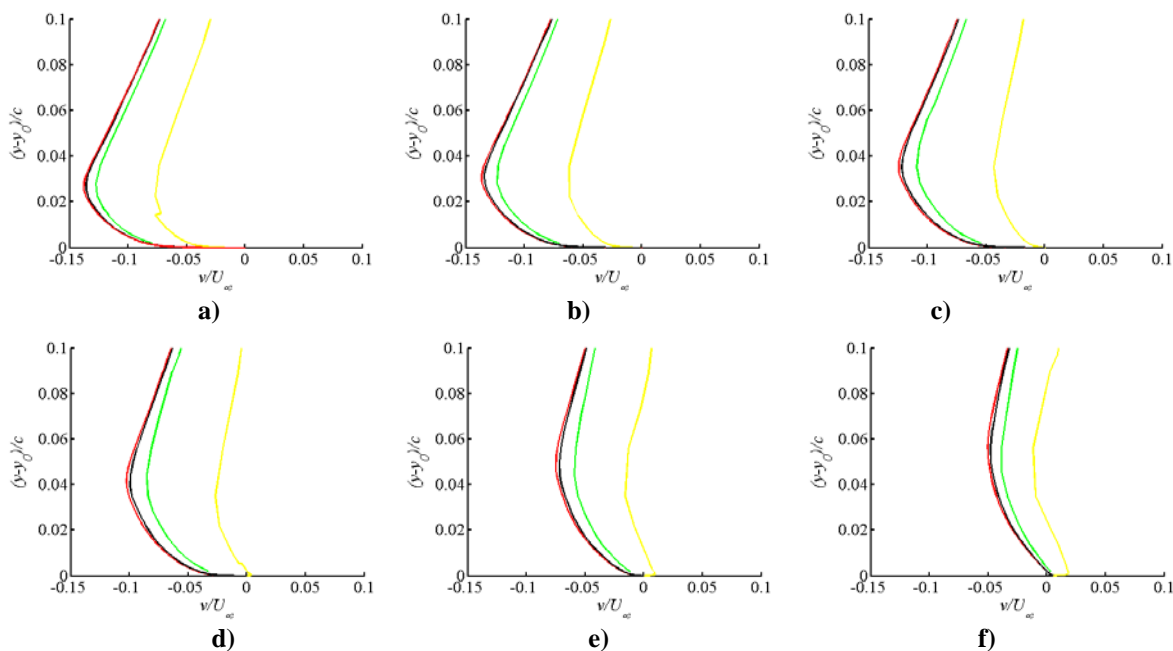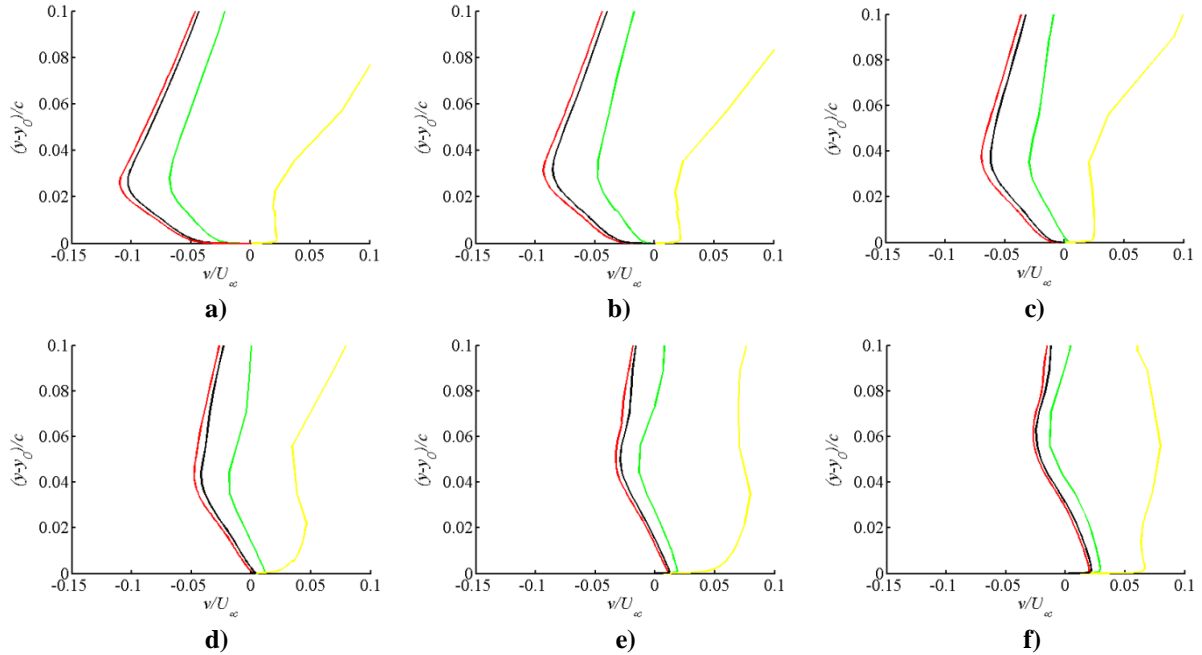
Figure 5. The transverse velocity profiles at a) x/c =0.6753, b) x/c =0.7308, c) x/c=0.7863, d) x/c=0.8418, e) x/c=0.8973 and, d) x/c=0.9528 obtained with the k-ω[6,7] model on different grids (notations as in Fig. 3).

5

American Institute of Aeronautics and Astronautics

Figure 6. The transverse velocity profiles at a) x/c =0.6753, b) x/c =0.7308, c) x/c=0.7863, d) x/c=0.8418, e) x/c=0.8973 and, d) x/c=0.9528 obtained with Menter's SST model[8] on different grids (notations as in Fig. 3).
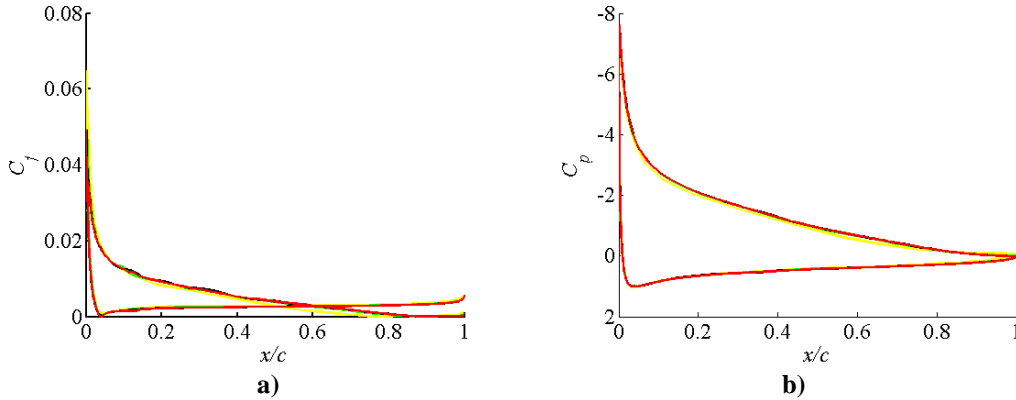

Figure 7. Results of the grid sensitivity analysis for a) skin friction coefficient and b) pressure coefficient obtained with the k-ω[6,7] model (notations as in Fig. 3).

All results in Figs. 11-13 are obtained on the grid 897×257. Profiles in Figs. 11 and 12 are along the line probes extended normally from the airfoil surface at locations where experimental[14,15] and CFL3D and FUN3D data[13] are available. In the figures, symbols correspond to experimental data, solids lines are the results of simulations with OpenFOAM, and dashed lines are data from Ref. 13. In Figure 13, circles correspond to experimental data and lines are computational profiles.

The streamwise velocity profiles obtained with Menter's SST model[8] implemented in OpenFOAM are closer to the experimental data than the results obtained with the high-fedility NASA codes (Fig. 11a). The transverse velocity profiles are not well predicted with this model (Fig. 12a). The OpenFOAM profiles obtained with this model did not converge to the solutions obtained with the NASA codes. In contrast, the results obtained with the k-ω model[6,7] implemented in OpenFoam converged to the data obtained with the NASA codes (Figs. 11b and 12b). However, results for both velocity components obtained with the k-ω model[6,7] are in less agreement with the experiemntal data than those obtained with Menter's SST model[8]. OpenFOAM produced the same friction coefficient as the NASA codes with both turbulence models (Fig. 13).
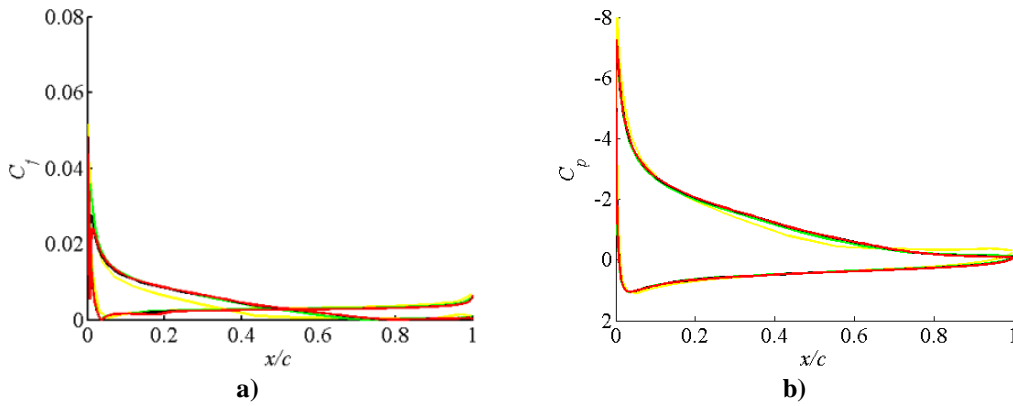
Figure 8. Results of the grid sensitivity analysis for a) skin friction coefficient and b) pressure coefficient obtained with Menter's SST model[8] (notations as in Fig. 3).

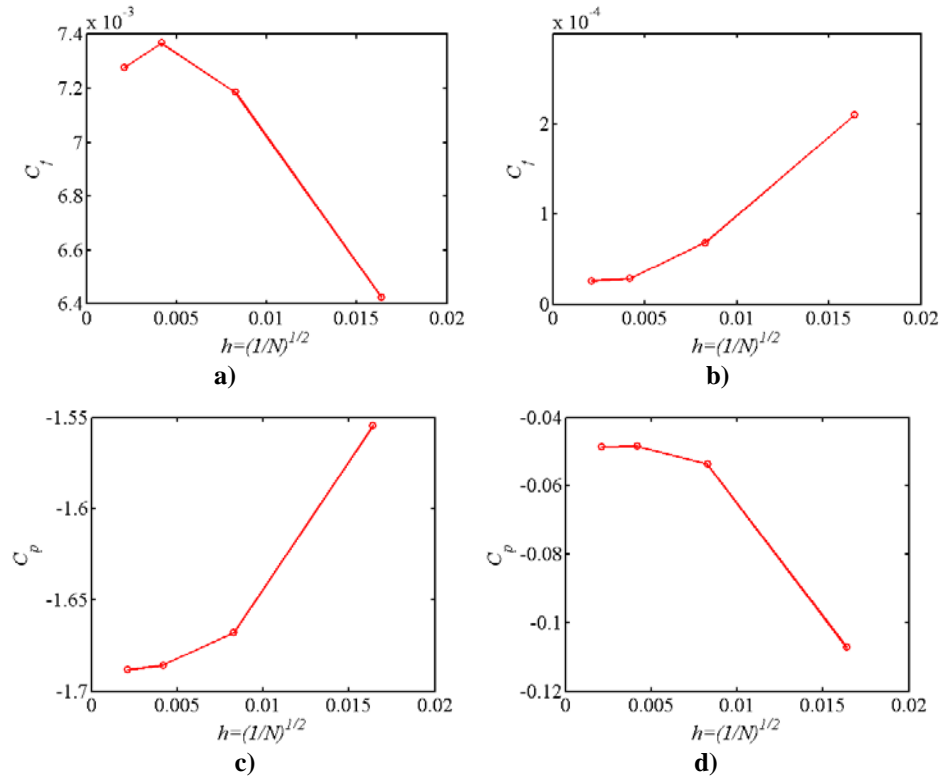**Figure 9. Richardson extrapolation analysis for the friction coefficient at a) x/c = 0.3 and b) x/c = 0.9, and the pressure coefficient at c) x/c = 0.3 and d) x/c = 0.9 obtained with the k-ω[6,7] turbulence model.**

The second set of simulation parameters based on Wadcock[16] was only used in simulations on the finest grid grid 897×257. Results are presented in Fig. 14. Menter's SST[8] turbulence model results are in a better agreement with the LES profiles[17] and the experimental data[16].

Overall, results from our previous[24] and current analyses of the OpenFOAM capabilities in wall-bounded flows show that when a turbulence model is implemented correctly in this software, results of simulations obtained with OpenFOAM are in close agreement with those obtained with the high-fidelity NASA codes. Thus, the code is suitable for validating other turbulence models, such as Reynolds Stress Transport models, for example.
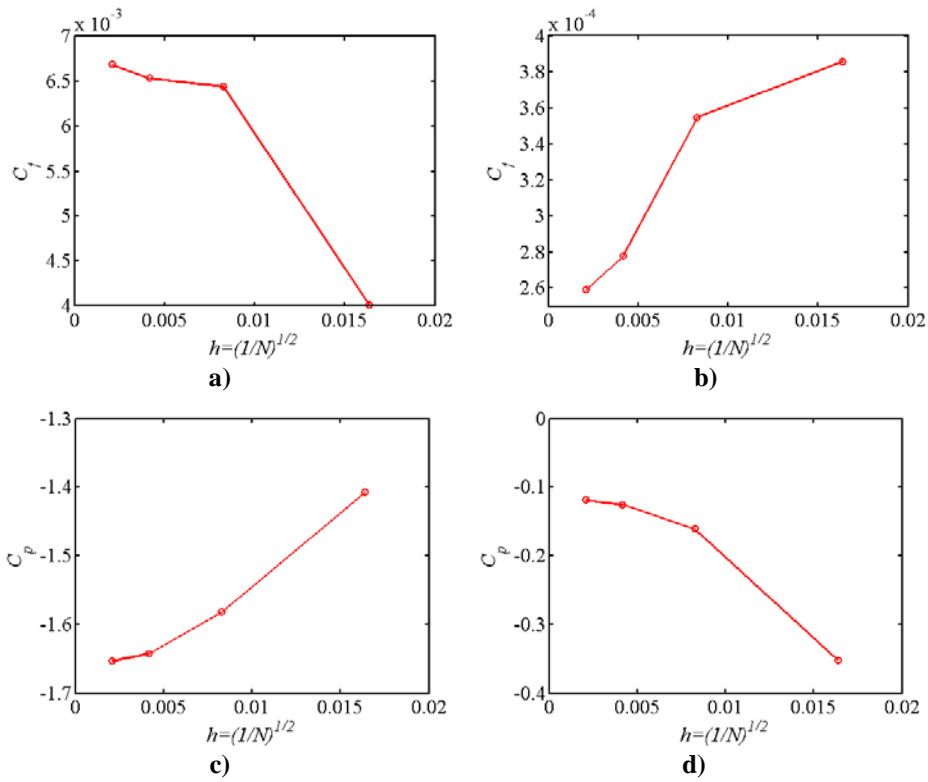
Figure 10. Richardson extrapolation analysis for the friction coefficient at a) x/c = 0.3 and b) x/c = 0.9, and the pressure coefficient at c) x/c = 0.3 and d) x/c = 0.9 obtained with Menter's SST model[8].
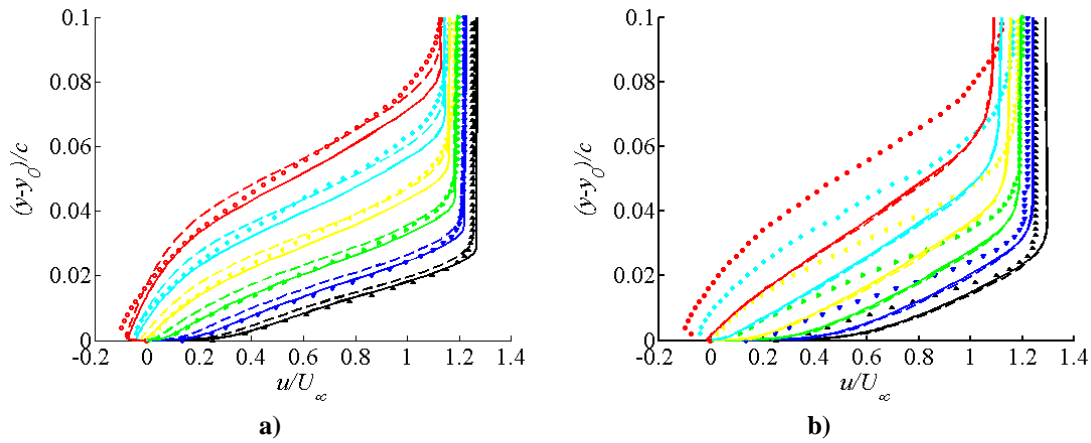

Figure 11. Streamwise velocity profiles for a flow over the NACA 4412 airfoil obtained on the grid 897×257 with a) Menter's SST[8] and b) k-ω[6,7] turbulence models. Notations: experimental data ▲ x/c=0.6753, ▼ x/c=0.7308, ► x/c=0.7863, ◄ x/c=0.8418, ♦ x/c=0.8973, ● x/c=0.9528; computational profiles: - - - FUN3D and CFL3D, — OpenFOAM.
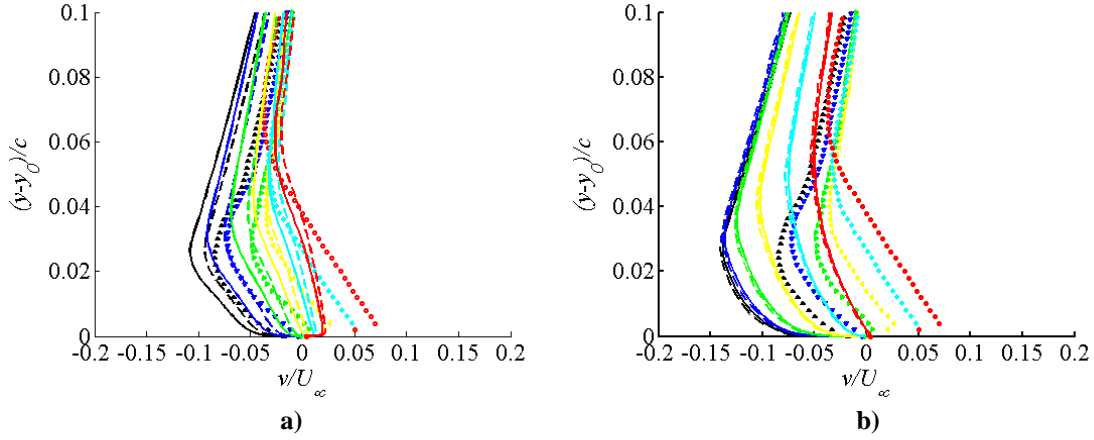
Figure 12. Transverse velocity profiles for a flow over the NACA 4412 airfoil obtained on the grid 897×257 with a) Menter's SST[8] and b) k-ω[6,7] turbulence models (notations as in Fig. 11).
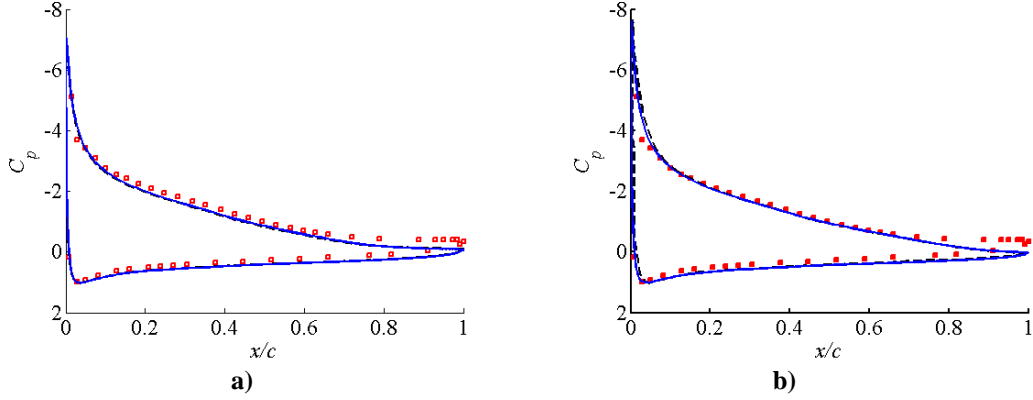

Figure 13. Pressure coefficient for a flow over the NACA 4412 airfoil obtained on the grid 897×257 with a) Menter's SST[8] and b) k-ω[6,7] turbulence models. Notations: ■ experimental data, - - - FUN3D and CFL3D, — OpenFOAM.

Two formulations of the Launder-Reece-Rodi (LRR) model[9] with the Gibson-Launder wall corrections[10] are considered in the current study: the first formulation is the one originally implemented in OpenFOAM and referred as Gibson-Launder model there[12] (hereafter, OpenFOAM-LRR):

$$\frac{\partial R_{ij}}{\partial t} + U_k \frac{\partial R_{ij}}{\partial x_k} = P_{ij} + D_{ij} - \frac{2}{3}\delta_{ij}\varepsilon + \Phi_{ij1} + \Phi_{ij2} + \left(\Phi_{ij}^{w1} + \Phi_{ij}^{w2}\right)f(x_n), \tag{3}$$

$$P_{ij} = -\left(R_{ik}\frac{\partial U_j}{\partial x_k} + R_{jk}\frac{\partial U_i}{\partial x_k}\right),$$

$$D_{ij} = \frac{\partial}{\partial x_k}\left[\left(v + \frac{v_t}{\sigma_R}\right)\frac{\partial R_{ij}}{\partial x_i}\right],$$

$$\Phi_{ij1} = -C_1\frac{\varepsilon}{k}\left(R_{ij} - \frac{2}{3}\delta_{ij}\varepsilon\right),$$

$$\Phi_{ij2} = -C_2 \left(P_{ij} - \frac{1}{3} P_{kk}\delta_{ij}\right),$$

$$\Phi_{ij}^{w1} = C_1^w \frac{\varepsilon}{k} \left[R_{mk}n_k n_m \delta_{ij} - \frac{3}{2}(R_{ik}n_k n_j + R_{jk}n_k n_i)\right],$$

$$\Phi_{ij}^{w2} = C_2^w \left[\Phi_{mk2}n_k n_m \delta_{ij} - \frac{3}{2}(\Phi_{ik2}n_k n_j + \Phi_{jk2}n_k n_i)\right],$$

$$\frac{\partial \varepsilon}{\partial t} + U_i \frac{\partial \varepsilon}{\partial x_i} = \frac{\partial}{\partial x_i}\left[\left(\nu + \frac{\nu_t}{\sigma_\varepsilon}\right)\frac{\partial \varepsilon}{\partial x_i}\right] + C_{\varepsilon 1}\frac{\varepsilon}{k}P - C_{\varepsilon 2}\frac{\varepsilon^2}{k}, \quad (4)$$

$$f(x_n) = \frac{C_\mu^{3/4} k^{3/2}}{\kappa \varepsilon x_n}, P = \frac{1}{2}P_{kk}.$$

Table 1. Model coefficients for OpenFOAM-LRR model[12].

C_μ	κ	σ_ε	σ_R	$C_{\varepsilon 1}$	$C_{\varepsilon 2}$	C_1	C_2	C_1^w	C_2^w
0.09	0.41	1.3	0.81967	1.44	1.92	1.8	0.6	0.5	0.3

The second formulation is the one used in Ref. 11 (hereafter, modified LRR-GL). Only equations that are different from OpenFOAM-LRR are shown for this version:

$$\frac{\partial R_{ij}}{\partial t} + U_k \frac{\partial R_{ij}}{\partial x_k} = P_{ij} + D_{ij} - \varepsilon_{ij} + \Phi_{ij1} + \Phi_{ij2} + \left(\Phi_{ij}^{w1} + \Phi_{ij}^{w2}\right)f(x_n), \quad (5)$$

$$\varepsilon_{ij} = \frac{2}{3}\tilde{\varepsilon}\delta_{ij} + 2\nu \frac{R_{ij}}{x_n^2},$$

$$f(x_n) = \frac{1}{5}\frac{k^{\frac{3}{2}}}{\varepsilon x_n},$$

$$\frac{\partial \tilde{\varepsilon}}{\partial t} + U_i \frac{\partial \tilde{\varepsilon}}{\partial x_i} = \frac{\partial}{\partial x_k}\left[\left(\nu\delta_{kl} + C_\varepsilon \frac{k}{\varepsilon}R_{kl}\right)\frac{\partial \tilde{\varepsilon}}{\partial x_l}\right] + \frac{\tilde{\varepsilon}}{k}(C_{\varepsilon 1}P - C_{\varepsilon 2}^*\tilde{\varepsilon}) - \frac{2\nu\tilde{\varepsilon}}{x_n^2}f_1, \quad (6)$$

$$C_{\varepsilon 2}^* = C_{\varepsilon 2}f_2, \quad f_1 = e^{\left[-\frac{x_n u_\tau}{2\nu}\right]}, \quad f_2 = 1 - \frac{2}{9}e^{\left[-\left(\frac{k^2}{6\nu\varepsilon}\right)^2\right]}.$$

Table 2. Model coefficients for LRR-GL model[11].

C_ε	C_s	$C_{\varepsilon 1}$	$C_{\varepsilon 2}$	C_1	C_2	C_1^w	C_2^w
0.15	0.2	1.44	1.92	1.8	0.6	0.3	0.3

In the LRR-GL model, $\tilde{\varepsilon}$ has the zero value at the wall.

Results obtained with the two LRR versions are presented in Figs. 15-17. Simulations were conducted on all four grids, but the steady solution could not be obtained on the finest grid 897×257. With both model formulations, the converged solutions were obtained on this grid, but they were unsteady ones. No such problem occurred when coarser grids were used. This issue has to be investigated further.

In Figure 15, results are shown for the zero angle of attack obtained on the grid 449×129; all other flow parameters are as in Refs. 13-15. Simulations at this angle of attack were conducted to verify models' implementation in OpenFOAM. In the figure, data from Wadcock[15] and Pinkerton[23] are provided for comparison. The Reynolds number for the data from Ref. 23 is 3×10^6, whereas in Wadcock[15], Re = 1.52×10^6. Both considered LRR versions accurately predict the pressure coefficient at this angle of attack following close Pinkerton's modified theory. At higher angle of attack (Fig. 16), both LRR versions give comparable results, but they are somewhat less
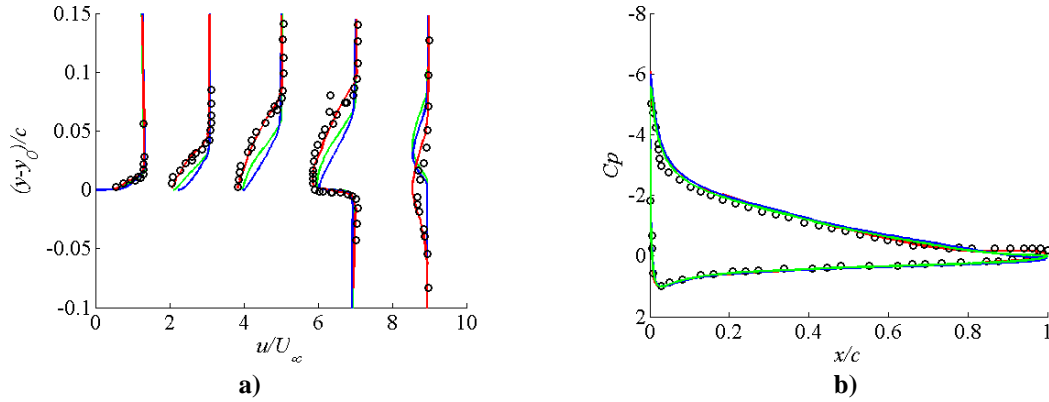
10
American Institute of Aeronautics and Astronautics

a) **b)**

Figure 14. Results of simulations of a flow over the NACA 4412 airfoil corresponding to the experimental data of Wadcock[16]: a) from left to right, streamwise velocity at x/c = 0.529, 0.815, and 0.952, and velocity normal to the tunnel axis in the wake at x_w/c = 0.007, 0.282 (profiles are shifted by 0, 2, 4, 6, and 8 along the abscissa); b) pressure coefficient. Notations: ○ experimental data, —— LES[17], —— Menter's SST model[8], —— k-ω[6,7] model.
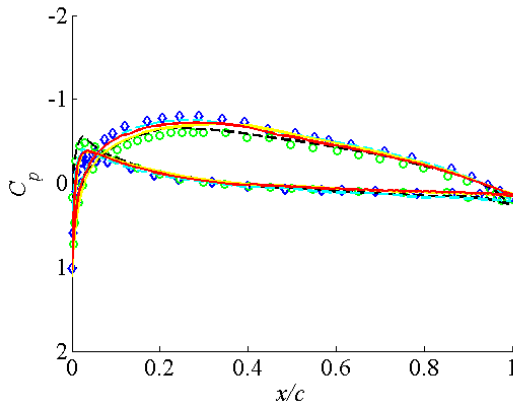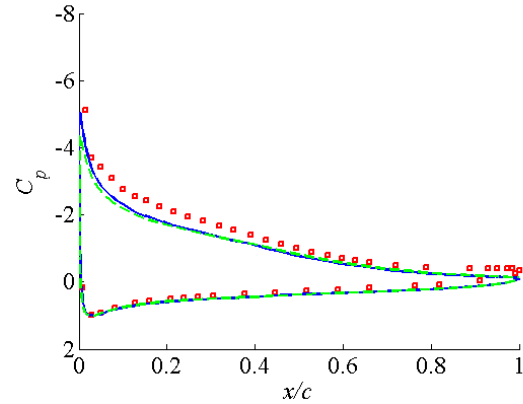

Figure 15. Pressure coefficient for a flow over the NACA 4412 airfoil at the zero angle of attack obtained on the grid 449×129. Notations: ◆ Wadcock[16], ● Pinkerton[23], - - - Pinkerton's modified theory[23], - - - Pinkerton's theory[23], —— OpenFOAM-LRR, ——LRR-GL.

Figure 16. Pressure coefficient for a flow over the NACA 4412 airfoil at the 13.87[0] angle of attack obtained on the grid 449×129. Notations: ■ experimental data[15], - - - OpenFOAM-LRR, —— LRR-GL.

accurate than the results from the two-equation models (Fig. 13). Similar conclusions can be made about velocity profiles predicted with the two LRR versions (Fig. 17). No attempt to modify the values of model coefficients was made in the current study to improve the LRR performance.

B. Circular Cylinder

Flow simulations around a 2D circular cylinder were conducted with two-equation turbulence models: Wilcox's 2006 k-ω model[6,7] and Menter's SST model[8] implemented in OpenFOAM in their standard formulations[13]. Table 3 provides a summary of some results obtained with the two models along with the results from other studies: experiments[18], LES[20], URANS[19,20], and DES[21,22].

The drag coefficients produced by the k-ω[6,7] and Menter's SST[8] turbulence models are significantly underpredicted to compare with the experimental data[19] and with the data obtained in other simulations[19-22]. From the two models, Menter's SST[8] turbulence model gives a better estimate of the drag coefficient. The separation angle, ϕ, on the top of the cylinder is determined by the angle θ, when the drag coefficient is zero. The k-ω[6,7] turbulence model outperforms Menter's SST[8] model for this parameter when simulation results are compared with the experimental data. Results from all simulations disagree with the experimental value for this angle.
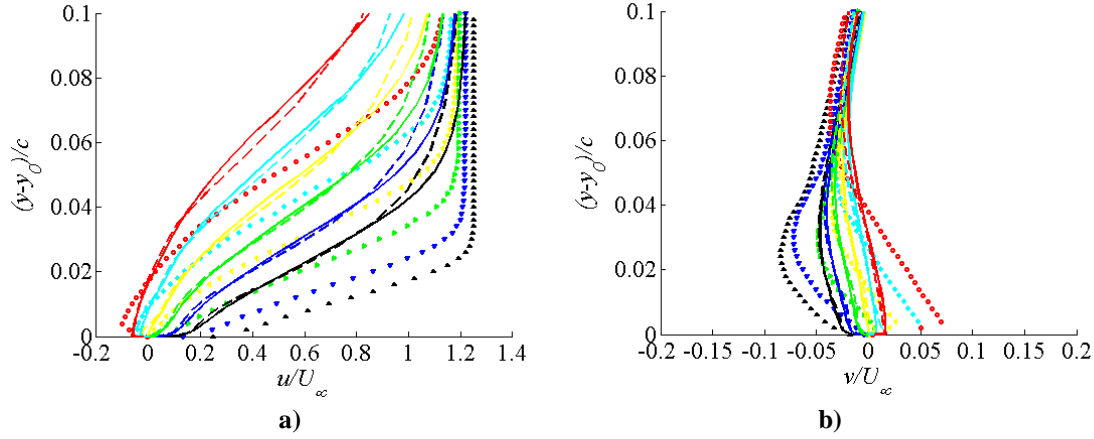
Figure 17. Velocity profiles for a flow over the NACA 4412 airfoil at the 13.87^0 angle of attack obtained on the grid 449×129: a) streamwise component and b) transverse component. Notations: experimental data[15] at locations ▲ x/c=0.6753, ▼ x/c=0.7308, ▶ x/c=0.7863, ◀ x/c=0.8418, ◆ x/c=0.8973, ● x/c=0.9528; - - - OpenFOAM-LRR, — LRR-GL.

The recirculation zone, L_r, is defined as the region in the middle of the wake where the streamwise velocity is negative. To compare with the results from other studies, k-ω[6,7] and Menter's SST[8] models predict a larger recirculation zone, with the SST model[8] producing the smaller recirculation zone than the k-ω[6,7] model does.

Table 3. Summary of cylinder results.

Turbulence Model/ Method	Re	C_D	ϕ	L_r/D
k-ω[6,7] (OpenFOAM)	3×10^6	0.271	110.8°	1.982
k-ω[6,7] (OpenFOAM)	3.6×10^6	0.253	111.3°	1.936
Menter SST[8] (OpenFOAM)	3×10^6	0.386	105.4°	1.649
Menter SST[8] (OpenFOAM)	3.6×10^6	0.366	107°	1.574
Travin et al.[21] (DES)	3×10^6	0.41, 0.51	106°, 111°	1.0, 1.0
Lo et al.[22] (DES)	3.6×10^6	0.576, 0.535	118°, 119°	0.35, 0.32
Ong et al.[19] (URANS)	3.6×10^6	0.4573	114°	~
Achenbach[18] (Experiment)	3.6×10^6	0.76	115°	~
Catalano[20] (LES, URANS)	1×10^6	0.31, 0.40	103°, ~	1.04, 1.37

In Figure 18, variations of friction and pressure coefficients on the cylinder surface are shown with respect to the angle θ. All simulations overpredict the friction coefficient at $\theta < 100^0$ and underpredict the pressure coefficient at $\theta > 100^0$. The two-equation models produce results close to the DES data[21].

Velocity profiles at different locations are shown in Figs. 19 and 20. No experimental data are available for comparison. The two-equation turbulence models generate qualitatively similar profiles to those obtained in LES and URANS simulations. The discrepancy between the results increases in the cylinder wake. In Figure 21, the mid-wake velocity profiles in the streamwise direction are shown. No reference data are available for this parameter.

V. Conclusion

Flow simulations around 2D streamlined bodies were conducted with turbulence models implemented in OpenFOAM. Simulations of a flow around the NACA 4412 airfoil with two-equation turbulence models – Wilcox's 2006 k-ω model[6,7] and Menter's SST model[8] –demonstrated that when a model is implemented correctly in this software, results of simulations obtained with OpenFOAM are in close agreement with those obtained with the high-fidelity NASA codes CFL3D and FUN3D . This result is in agreement with our previous study[24]. For the airfoil flow simulations, it was found that the results obtained with Menter's SST model[8] are in closer agreement with experimental data than those produced with the k-ω[6,7] turbulence model. The grid convergence study showed that the grid 897×257 has sufficient resolution for generating grid-independent solutions.

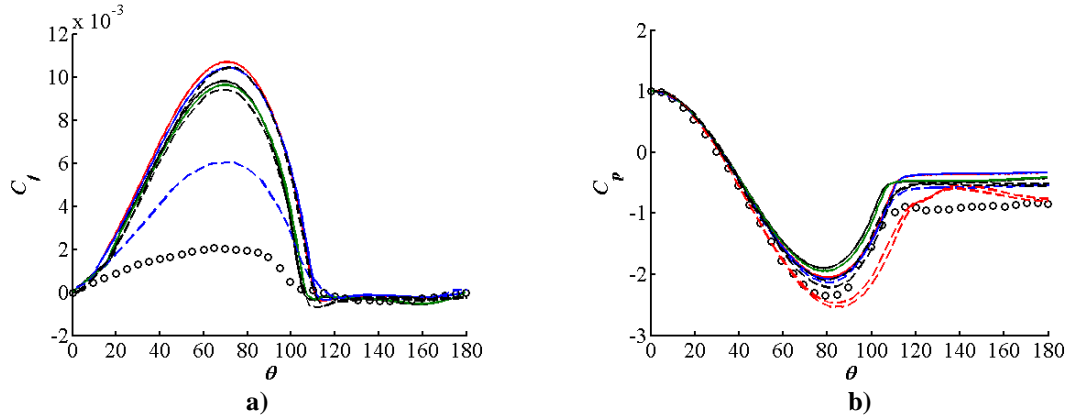**Figure 18. A flow around a 2D cylinder: a) friction coefficient, b) pressure coefficient. Notations: ⎯ Menter's SST[8] model at Re = 3×10^{6}, ⎯ Menter's SST[8] model at Re = 3.6×10^{6}, ⎯ k-ω[6,7] model at Re = 3×10^{6}, ⎯ k-ω[6,7] model at Re = 3.6×10^{6}, - - - URANS of Ong et al.[19] at Re = 3.6×10^{6}, - - - DES of Traven et al.[21] at Re = 3×10^{6}, - - - DES of Lo et al.[22] at Re = 3.6×10^{6}, ○ experimental data[18].**
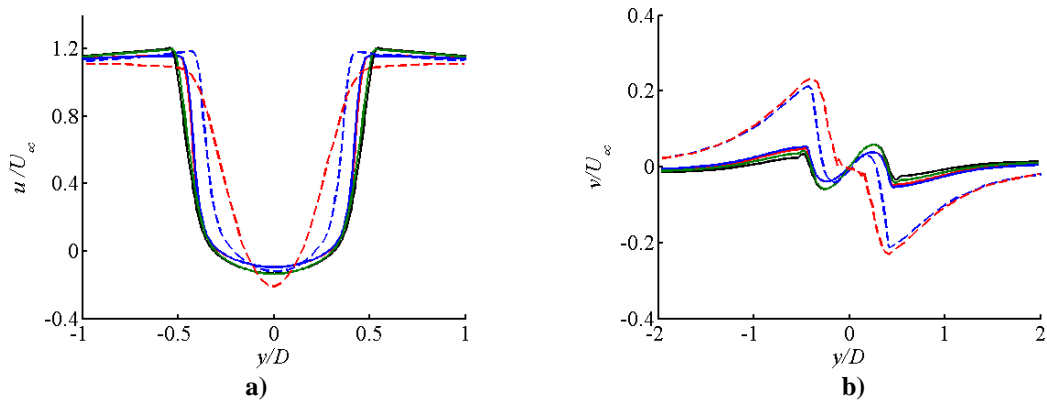

Figure 19. Velocity profiles in a flow around a cylinder along a vertical probe at x/D = 0.75: a) streamwise velocity, u, b) transverse velocity, v. Notations: ⎯ Menter's SST[8] model at Re = 3×10^{6}, ⎯ Menter's SST[8] model at Re = 3.6×10^{6}, ⎯ k-ω[6,7] model at Re = 3×10^{6}, ⎯ k-ω[6,7] model at Re = 3.6×10^{6}, - - - URANS Catalano et al.[20] at Re = 1×10^{6}, - - - LES Catalano et al.[20] at Re = 1×10^{6}.
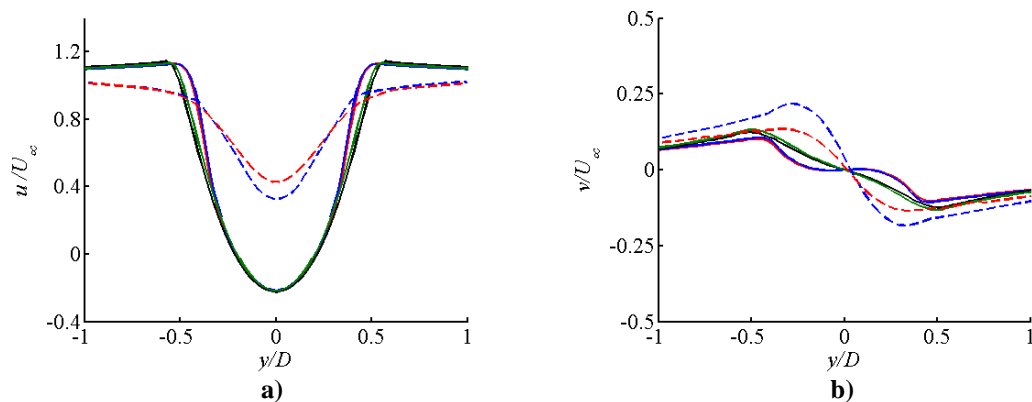

Figure 20. Velocity profiles in a flow around a cylinder along a vertical probe at x/D = 1.5 a) streamwise velocity, u, b) transverse velocity, v (notations as in Fig. 19).

American Institute of Aeronautics and Astronautics

Simulations around the NACA 4412 airfoil were also conducted with two versions of the LRR Reynolds Stress Transport model implemented in OpenFOAM. Although no version produced results in a better agreement with experimental data than the two-equation models did, further tuning the model coefficients may improve model's predictions.

Flow simulations around a 2D circular cylinder were conducted with the same two-equation turbulence models as used in the airfoil flow simulations. Results obtained with the two models are in close agreement with the DES[21] results for friction and pressure coefficients. Neither the two-equation turbulence models nor other simulation techniques[19-22] predicted the flow features accurately.
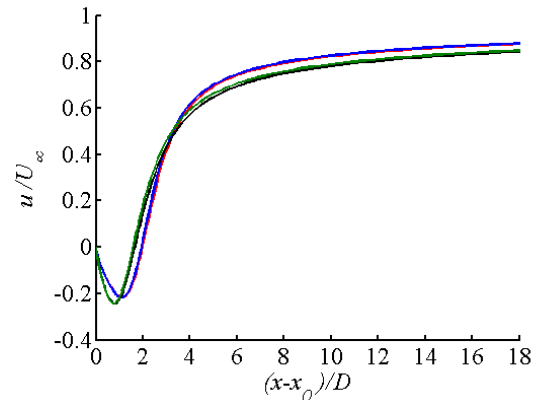

Figure 21. The mid-wake velocity profiles in the streamwise direction. Notations: — Menter's SST[8] model at Re = 3×10^6, — Menter's SST[8] model at Re = 3.6×10^6, — k-ω[6,7] model at Re = 3×10^6, — k-ω[6,7] model at Re = 3.6×10^6.

Acknowledgments

References

[1]Airfoil Investigation Database. URL: http://www.airfoildb.com/foils/325

[2]CFD Validation of Synthetic Jets and Turbulent Separation Control, NASA Langley. URL: http://cfdval2004.larc.nasa.gov

[3]11th ERCOFTAC/IAHR Workshop on Refined Turbulence Modelling, April 7-8, 2005, Chalmers Univ. of Technology, Sweden

[4]12th ERCOFTAC/IAHR Workshop on Refined Turbulence Modelling, October 12-13, 2006, Institute for Fluid Mechanics and Technical Acoustics, Technical University of Berlin, Germany

[5]V&V I: Code Verification and Solution Verification & Validation Workshop at ECCOMAS CFD 2010, June 14-17, 2010, Lisbon, Portugal.

[6]Wilcox, D. C., "Turbulence Modeling for CFD, 3rd edition," DCW Industries, Inc., La Canada CA, 2006.

[7]Wilcox, D. C., "Formulation of the k-omega Turbulence Model Revisited," *AIAA Journal*, Vol. 46, No. 11, 2008, pp. 2823-2838.

[8]Menter, F. R., "Two-Equation Eddy-Viscosity Turbulence Models for Engineering Applications," *AIAA Journal*, Vol. 32, No. 8, August 1994, pp. 1598-1605.

[9] Launder, B. E., Reece, G. J., Rodi, W., "Progress in the development of a Reynolds stress turbulent model," *J. Fluid Mech.*, Vol. 68, 1973, pp. 537-566.

[10]Gibson, M. M., Launder, B. E., "Ground effects on pressure fluctuations in the atmospheric boundary layer," *J. Fluid Mech.*, Vol. 86, 1978, pp. 491-511.

[11]Kurbatskii, A. F., Poroseva, S. V., "Modelling turbulent diffusion in a rotating cylindrical pipe flow," *Int. J. Heat and Fluid Flow*, 20(3), 1999, pp. 341-348.

[12]OpenFOAM, Open-source Field Operation and Manipulation, Software Package, Ver. 2.2.0, 2011. URL: http://www.openfoam.com

[13]Turbulence Model Benchmarking Working Group Turbulence Modeling Resource, NASA Langley. URL: http://turbmodels.larc.nasa.gov/flatplate.html

[14]Coles, D. and Wadcock, A. J., "Flying-Hot-Wire Study of Flow Past an NACA 4412 Airfoil at Maximum Lift," *AIAA Journal*, Vol. 17, No. 4, April 1979, pp. 321-329

[15]Wadcock, A. J., "Structure of the Turbulent Separated Flow Around a Stalled Airfoil," *NASA-CR-152263*, February 1979.

[16]Wadcock, A. J., "Investigation of low-speed turbulent separated flow around airfoils," NASA Contractor ReportNo. 177450, 1987.

[17] Park, G.I. and Moin, P, "An improved dynamic non-equilibrium wall-model for large eddy simulation," *Physics of Fluids*, Vol. 26, Jan. 2014.

[18]Achenbach, E. "Distribution of local pressure and skin friction around a circular cylinder in cross-flow up to Re = 5×10^6," *Journal of Fluid Mechanics*, Vol. 34, Part 4, 1968, pp. 625-639.

[19]Ong, M. C., Utnes, T., Holmedal, L. E., Myrhaug, D., Pettersen, B., "Numerical simulation of flow around a smooth circular cylinder at very high Reynolds numbers," *Marine Structures*, Vol. 22, Part 2, 2009, pp. 142-153.

[20]Catalano, P., Wang, M., Iaccarino, G., Moin, P., "Numerical simulation of the flow around a circular cylinder at high Reynolds numbers," *International Journal of Heat and Fluid Flow*, Vol. 24, 2003, 463-469.

[21]Travin, A., Shur, M., Strelets, M., Spalart, P., "Detached-Eddy Simulations Past a Circular Cylinder," *Flow, Turbulence and Combustion*, Vol. 63, 1999, pp 293-313.

[22]Lo, S.-C., Hoffmann, K. A., Dietiker, J.-F., "Numerical investigation of high Reynolds number flows over square and circular cylinders," *Journal of Termophysics and Heat Transfer*, Vol. 19, No. 1, 2005, pp. 72-80.

[23]Pinkerton, R.M., "Calculated and measured pressure distribution over the midspan section of the N.A.C.A. 4412 airfoil," *National Advisory Committee for Aeronautics,* Report No. 563, 1936.

[24]Gomez, S., Graves, B.J., Poroseva, S.V., "On the Accuracy of RANS Simulations of 2D Boundary Layers with OpenFOAM," *Proc. AIAA Aviation and Aeronautics Forum and Exposition*, Atlanta, GA, June 16-20, 2014.